

Droplet morphology simulation with SPH: A simple method of implementing contact angles

Xiangwei Dong¹

¹Department of Engineering Mechanics, China University of Petroleum(East China), Qingdao, China

*Presenting author: dongxw139@163.com

†Corresponding author: dongxw139@163.com

Abstract

The use of the smoothed particle hydrodynamics (SPH) method to simulate the surface tension effects requires an efficient description of the three phase contact line among liquid, gas, and solid. In this study, based on the continuum surface force (CSF) model, the virtual interface method is proposed to implement the contact angle in the SPH multiphase simulation. The first step is to create the virtual gas-liquid interface at the triple contact point according to the desired contact line. Then, the adjusting force acting on the fluid of the triple line can be expressed as the function of the interface curvature, which can gradually adjust the dynamic contact line towards the desired contact angle. The proposed method is successfully applied to simulate the droplet morphologies on smooth and roughness surfaces. The numerical results are in agreement with the previous analytical solutions. These analyses hold great potentials in bio-inspired superhydrophobic surfaces, oil displacement, microfluidics, and ore floatation, etc.

Keywords: **Smoothed particle hydrodynamics (SPH); virtual interface method; equilibrium contact angle; droplet morphology; roughness surface substrate.**

1. Introduction

Surface tension and contact line dynamics play a major role in many industrial fields, including inkjet printing[1], powder agglomeration[2] and microfluidics[3], etc. These phenomena also occur in the nature world, such as the superhydrophobic effect of the surface of the lotus leaf[4], nutrition transportation in plants via Phloem and Xylem tissues[5], and some aquatic creatures walking on water[6]. Therefore, much effort has been devoted to explore this area, both from experimental and numerical viewpoints. It should be mentioned that it is not easy to perform experiments in some extreme conditions, and thus numerical simulation must be the necessary approach, which can shorten time and lower expenses. A main task is to develop the numerical model in consideration of the surface tension.

Currently, two common computational fluid dynamics (CFD) approaches are used in multiphase simulations with surface tension effects being considered. The first one is the volume-of-fluid method (VOF)[7] which belongs to grid-based methods, and the second one can be grouped into the particle-based Lagrangian methods, such as the smoothed particle

hydrodynamics (SPH) method[8]. The SPH method was originally proposed to simulate the astrophysical phenomena[9] and then widely used in the simulation of hydrodynamics[10] and solid mechanics[11]. Up to now, the SPH method has also been applied in the simulation of multiphase flows[12–18]. And the Lagrangian nature of SPH makes it a good option for simulating complex multiphase problems.

In SPH multiphase simulations, there exist two ways to implement the surface tension. The first is based on the van der Waals force implemented through particle-particle interactions[20]. Surface tension effects can be simulated by adding the van der Waals force in the pressure term. Tartakovsky and Meakin[21] combined the standard SPH equations with pairwise fluid-solid particle-particle interactions to simulate capillarity. In their work, the simulation of contact lines is realized through the interplay between the pinning forces provided by particle-particle interactions, and driving forces from the gravity. The second method is the continuum surface force (CSF) method, where the surface tension is expressed as a function of the interface normal vector, curvature and surface tension coefficient[22]. The CSF method was first implemented in SPH by Morris[23] in use of the color function for the interface tracking. It is widely accepted that the CSF method is more perceptible than the first method because its formulation contains the surface tension coefficient, which is convenient to control the surface tension according to actual physics.

The implementation of the CSF method requires proper boundary conditions to account for the three-phase contact. Liu and Liu[24] simulated the micro-channel flow adopting an asymmetric SPH model, and the simulation of the contact line with solid surface is realized based on the normal correction method proposed by Brackbill et al.[22]. Hu and Adams[25] developed a multi-phase SPH method from a particle smoothing function in which the neighboring particles only contribute to the specific volume but not density, and this method was used to simulate channel flow by using virtual particles to account for the wall-fluid interaction. But only the straight channel wall was considered. Das and Das proposed another method to handle the wall-fluid interaction, in which the equilibrium contact angle was simulated by incrementally translating particles in the triple contact region. In this method, a constant reconstruction of the triple line is required, and the method was only tested for smooth surfaces also. Breinlinger[28] proposed a smoothed normal correction method to modify the interface normal vectors near the triple line, and introduced an adjusting force to obtain the desired contact line position. Yeganehdoust[19] adopted a similar way to introduce the adjusting force, and proposed a new scheme to correct the normal vectors by re-assigning the color values of dummy particles for solid wall. However, the method needs additional fitting parameters to tune the result so that it is only applied to smooth surfaces. As we all know, most wetting and dewetting phenomena of solid materials are closely related to the micro-structures of their surfaces[29]. For example, the leaves of lotus can keep off rain drops due to its hierarchical surface structures. Inspired by the skill of superhydrophobicity of lotus, rough surfaces with appropriate wetting properties have various applications in industry, e.g., porous media, micro-fluidic devices, self-cleaning paints, and glass windows. Therefore, it is necessary to develop the numerical model for simulation of surface wetting for roughness surface, i.e., the surface with micro-structures.

Following the previous studies, and on the basis of the SPH multiphase algorithm and CSF model, a simple and deterministic method of implementing contact angle is proposed, which can effectively simulate the droplet morphology on the solid surface. In the method, dummy particles of solid wall are used to create the virtual gas-liquid interface near the triple line. Then, the adjusting force which is the function of the interface curvature is introduced to

adjust the dynamic contact line towards the desired contact angle. The method is suitable for both smooth surface and roughness surface substrates. Only two-dimensional problems will be considered in this paper, though the presented model and method can be extended to three-dimensional cases without too much efforts.

2. Model formulation

2.1 Field equations

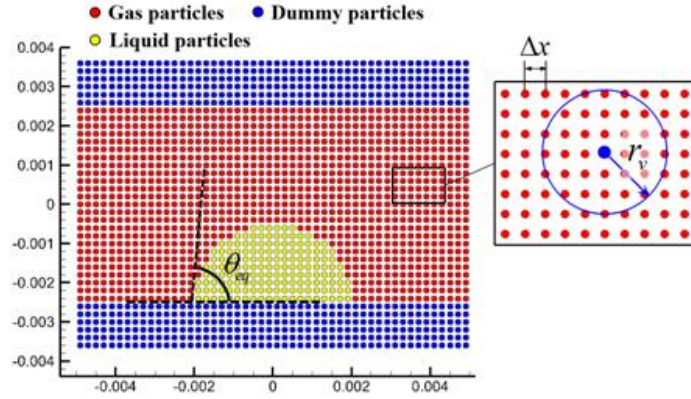


Figure 1 Modeling on a droplet

We first introduce the schematic of the computational model of a droplet deposited on a smooth surface. As shown in Figure 1, at the triple contact line, there is an angle between the liquid-gas interface and solid-liquid interface, which is termed as the Young's contact angle. In the two-dimensional case, the morphology of the droplet can be formulated by the elliptic integrals once the volume and Young's contact angle are given. Herein, we want to simulate the droplet configuration in use of the SPH method. As demonstrated in Figure 1, a computational domain is selected to include the droplet-substrate system. Then the domain is discretized by a finite number of particles, and each particle is assigned physical parameter values and certain volume.

In this study, the Navier–Stokes equation, in combination with the mass conservation equations, are adopted to describe the motion of the fluids, i.e. the gas and liquid. These field equations in Lagrangian view are expressed as follows[12]:

$$\frac{D\rho}{Dt} = -\rho\nabla \cdot \mathbf{u}, \quad (1)$$

$$\rho \frac{D\mathbf{u}}{Dt} = \nabla P + \mathbf{f}^V + \mathbf{f}^B + \mathbf{f}^S + \mathbf{f}^I, \quad (2)$$

where ρ is the mass density, t is the time variable, \mathbf{u} is the velocity, ∇P is the pressure gradient, \mathbf{f}^V , \mathbf{f}^B , and \mathbf{f}^S are the forces per unit mass, which correspond to the viscous force, body force (such as gravity) and surface tension force, respectively.

The fluid is considered as incompressible, so the viscous force per unit mass can be expressed as:

$$\mathbf{f}^V = \mu\nabla^2\mathbf{u}, \quad (3)$$

where μ is the dynamic viscous coefficient.

The surface tension force is computed using the continuum surface force (CSF) method[22]. According to the CSF method, f^S can be written as

$$\mathbf{f}^S = -\sigma\kappa\mathbf{n}\lambda, \quad (4)$$

where σ is the surface tension of the liquid, which is assumed as a constant, κ is the curvature of an arbitrary point in the interface, \mathbf{n} is the normal unit vector of the interface, and λ is a smeared delta function.

An equation of state is compensated to calculate the fluid pressure[10]:

$$P = \frac{c^2\rho_0}{\gamma} \left(\left(\frac{\rho}{\rho_0} \right)^\gamma - 1 \right) + P_b, \quad (5)$$

where c is the speed of sound, ρ_0 is the reference density of fluid, γ is a constant parameter[14], and P_b is the background pressure which helps to prevent the tensile instability, and also keep the particles distributed uniformly[13].

2.2 SPH discretization

Evidently, the analytical solutions of Eqs. (1), (2) and (5) are intractable, and thus the numerical approach is adopted. Firstly, these equations should be discretized based on the SPH method, where the computational domain is initialized by a series of uniformly distributed particles. Considering there is a high density ratio between the two fluids, Eqs. (7) and (8) are discretized in the form of[12]:

$$\rho_i = m_i \sum_j W_{ij}, \quad (6)$$

$$\rho_i \frac{D\mathbf{u}_i}{Dt} = \left(-\frac{1}{V_i} \sum_j (P_i V_i^2 + P_j V_j^2) \nabla_i W_{ij} \right) + \mathbf{f}_i^V + \mathbf{f}_i^B + \mathbf{f}_i^S, \quad (7)$$

where the subscripts i and j are the particle indices. The symbol $V_i = \frac{m_i}{\rho_i}$ is the volume of the i th particle, W_{ij} represents the renormalized Gaussian kernel function $W(\mathbf{r}_i - \mathbf{r}_j, h)$ [14], where \mathbf{r}_i is the position vector of the i th particle, and h is the smoothing length. In the simulation, the value of h is set as a constant, which reads: $h = 1.0\Delta x$, and Δx is the initial particle spacing.

The viscous force per unit mass is discretized by the following equation[30]:

$$\mathbf{f}_i^V = \sum_j \mu_{ij} \frac{v_i^2 + v_j^2}{V_i} \frac{(\mathbf{r}_i - \mathbf{r}_j) \cdot \nabla_i W_{ij}}{|\mathbf{r}_i - \mathbf{r}_j|^2 + (0.01h)^2} (\mathbf{u}_i - \mathbf{u}_j), \quad (8)$$

where $\mu_{ij} \left(= \frac{2\mu_i\mu_j}{\mu_i + \mu_j} \right)$ is the mean inter particle viscosity, μ_i and μ_j are the dynamic viscosity of the i th particle and the j th particle.

2.3 Surface tension modeling

According to the Eq. (4), the surface tension force is correlated with the interface normal vector and curvature, so these two parameters should be calculated first. In the two phase flow,

for the i th particle of fluid 1, if some particles of fluid 2 exist in the supporting domain of the i th particle, the surface tension force f_i^S can be expressed as[17]:

$$\mathbf{f}_i^S = -\sigma^{1-2}\kappa_i|\nabla C_i|\mathbf{n}_i, \quad (9)$$

where σ^{1-2} represents the surface tension between fluid 1 and 2. The parameter κ_i is the curvature of the i th particle which is located in the interface, and C is the so-called color function and is defined as a pairwise form[17]:

$$C_i^j = \begin{cases} \frac{2\rho_i}{\rho_i + \rho_j} & \text{if the phase of the } i\text{th particle is different from the } j\text{th particle} \\ 0 & \text{if the phase of the } i\text{th particle is the same with the } j\text{th particle} \end{cases} \quad (10)$$

The normal unit vector at the i th particle is calculated using the following equation:

$$\mathbf{n}_i = \frac{\nabla C_i}{|\nabla C_i|}, \quad (11)$$

where ∇C_i is the gradient of the color function and its expression is[17]

$$\nabla C_i = \frac{1}{V_i} \sum_j (V_i^2 + V_j^2) \frac{C_i^i + C_i^j}{2} \nabla_i W_{ij}. \quad (12)$$

Then, the curvature of the i th particle is calculated based on the results of normal unit vectors:

$$\kappa_i = -d \frac{\sum_j (\mathbf{n}_i - \varphi_i^j \mathbf{n}_j) \cdot \nabla_i W_{ij} V_j}{\sum_j |\mathbf{r}_i - \mathbf{r}_j| \cdot |\nabla_i W_{ij}| V_j}, \quad (13)$$

where φ_i^j is defined similar to the color function[17]:

$$\varphi_i^j = \begin{cases} -1 & \text{if the phase of the } i\text{th particle is different from particle } j \\ 1 & \text{if the phase of particle } i \text{ is the same with particle } j \end{cases} \quad (14)$$

The function of φ_i^j is to reverse the direction of the normal vector in the neighbouring phase.

2.4 Time-stepping scheme

A modified prediction-correction time-stepping scheme[14], which is proposed for multiphase droplet dynamics with high density ratio, is applied. The explicit time-stepping scheme is subject to the Courant-Friedrichs-Levy (CFL) condition for stability. The time step is determined according to the following criterion:

$$\Delta t_c = CFL_c \frac{h}{c + u_{max}}, \quad (15)$$

where CFL_c is the coefficient set as $CFL_c = 1.0$, u_{max} is the maximum velocity in the fluid field. Besides, the magnitude of the time step Δt is also determined based on the following criterions:

$$\Delta t_s = CFL_s \left(\frac{\rho h^3}{2\pi\beta} \right)^{1/2}, \quad (16)$$

$$\Delta t_\mu = CFL_\mu \frac{\rho h^2}{\mu}, \quad (17)$$

where the coefficients are set as $CFL_s = 0.5$, $CFL_\mu = 0.125$. The final time step is determined as $\Delta t = \min(\Delta t_c, \Delta t_s, \Delta t_\mu)$.

3. Contact angle implementation

In this section, the method of implementing contact angle is proposed to simulate the droplet morphology with the desired contact angle value. The equilibrium contact angle θ_{eq} are given as the input parameters.

3.1 Interfacial forces at the triple line

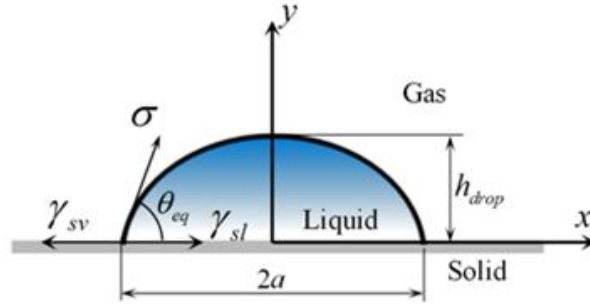


Figure 2 Illustration of interface tensions at the liquid-gas (σ), the solid-liquid (γ_{sl}), and the solid-gas (γ_{sv}) interface.

As shown in Figure 2, according to the Young's equation, the interfacial forces acting on the fluids of the droplet near the triple line can be expressed as:

$$\sigma \cos \theta_{eq} + \gamma_{sl} - \gamma_{sv} = 0, \quad (18)$$

where σ , γ_{sl} and γ_{sv} are the interface tensions at the liquid-gas, the solid-liquid, and the solid-gas interface, respectively.

In the dynamic simulation using SPH, if the instantaneous contact angle θ of a droplet is not consistent with the equilibrium contact angle θ_{eq} , the adjusting force should be introduced based on the following equation[28]:

$$F^a = \sigma(\cos \theta_{eq} - \cos \theta), \quad (19)$$

where F^a is the adjusting force, which is distributed into fluid particles near the triple line as the following equation:

$$\mathbf{F}^a = \sum_{j \in \Omega_{tri}} \mathbf{f}_j^a \quad (20)$$

where \mathbf{f}_j^a is the force acting on the j th particle of fluids; Ω_{tri} represents the domain near the triple line, and it is determined by the circle ($r_v = 3h$) centered on the triple contact point, as shown in Figure 3.

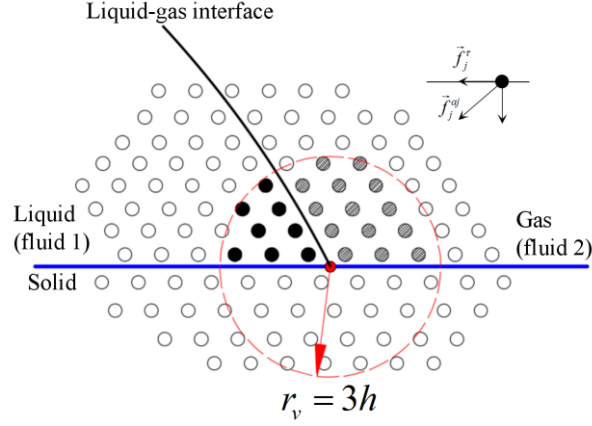


Figure 3 Shadowy circles mark the liquid particles located in the triple contact region. The adjusting force is distributed on these particles.

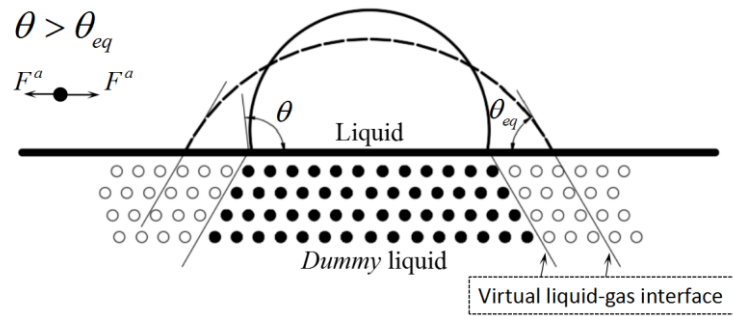
3.2 The virtual interface method

Here, we introduce the following equation to calculate the adjusting force:

$$\mathbf{f}_i^a = -\delta\kappa_i|\nabla C_i|\boldsymbol{\tau}_w, \quad (21)$$

where δ is an coefficient and is set equal to σ^{1-2} in this study, $\boldsymbol{\tau}_w$ is the tangential unit vector of the solid surface, κ_i and $|\nabla C_i|$ are calculated by the Eqs. (11), (12), and (13).

Before implementing Eq. (21), the dummy particles of the solid boundary should be treated first. As shown in Figure 4, the dummy particles are divided into two classes by the desired contact line. One part is attributed to type 1 and is given the same mass density as the liquid (as the solid circle marks in Figure 4), the other is attribute to type 2 which is given the same mass density as the gas. This is equivalent to create a dummy liquid-gas interface at the end of the real liquid-gas interface. Based on above treatment, the adjusting force (Eq. (21)) which has the same formulation as the surface tension force (Eq. (9)), is able to eliminate the concave or convex at the triple contact point. This is the basic principle of the virtual interface method.



(a)

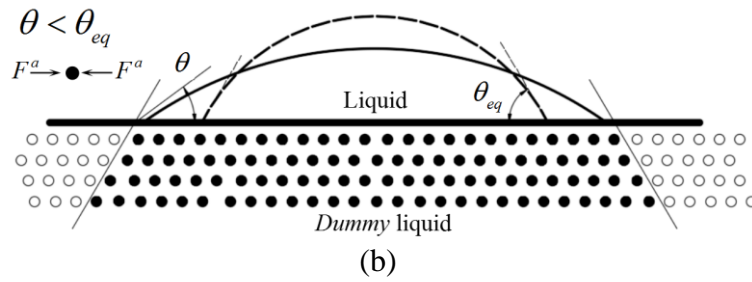


Figure 4 A droplet is deposited on the surface. Illustration of the distribution of dummy particles. (a) Non-equilibrium droplet with $\theta > \theta_{eq}$, (b) Non-equilibrium droplet with $\theta < \theta_{eq}$.

Figure 4 presents two situations that droplets are in non-equilibrium state with the instantaneous contact angle $\theta > \theta_{eq}$ and $\theta < \theta_{eq}$, respectively. If $\theta > \theta_{eq}$, as shown in Figure 4 (a), the adjusting force tends to stretch the droplet outwards due to the concave curvature at the triple contact point. While for the case of $\theta < \theta_{eq}$ (see Figure 4(b)), the adjusting force will stretch the droplet inwards. The equilibrium contact angle can be gradually approached under the effect of the adjusting force.

Figure 5 shows the distribution of interface normal vectors near the triple line. As shown in the Figure, for the case without using the virtual interface method, the fluid particles near the triple line have insufficient supporting particles because of the cutoff of the supporting domain by the wall boundary, which leads to incorrect results of normal vectors. Figure 5 (b) shows the results of normal vectors with the virtual interface method. The dash line represents the virtual liquid-gas interface which can be seen as the extension of the real liquid-gas interface. It shows that better distribution of normal vectors are obtained when the virtual interface method is used.

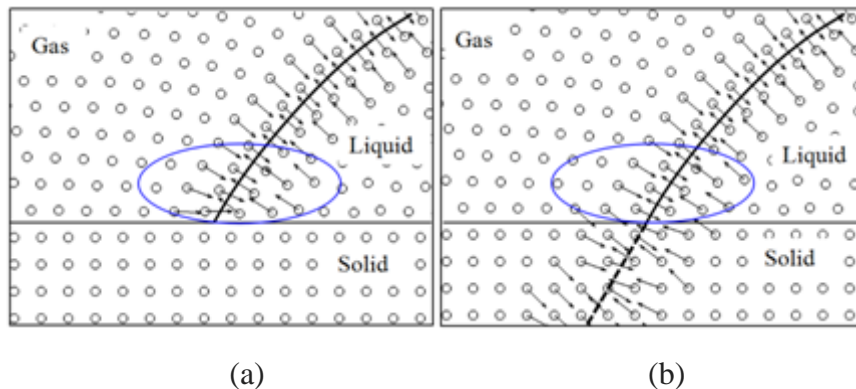


Figure 5 Normal vectors at the triple line (a) without using the virtual interface method and (b) using the virtual interface method

It can be seen that the first step of implementing the virtual interface method is to detect the triple contact points.

3.3 Implementation

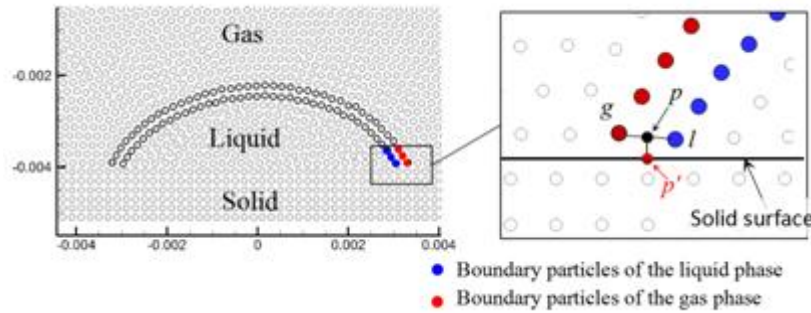


Figure 6 Detection of the triple contact point

For the two-dimensional problem, the triple contact point can be defined as the intersection between liquid-gas interface and solid surface. We propose the following procedure to identify the three-phase contact point in 2D as:

- 1) Search the boundary particles of the liquid and gas phases, respectively.
- 2) Identify two most downward interface particles close to solid surface, labeled as points g and l .
- 3) Take the mean coordinates of g and l as the intermediate point p , and then the projection of point p on the solid surface (p') is regarded as the triple contact point.

Following the method proposed by Dilts [32], the boundary particles can be detected by scanning the $3h$ -radius ($3h$ is the radius of the support domain) circle around an SPH particle. If the circle of the SPH particle is not completely covered by the circles of its neighbors, this particle is labeled as a boundary particle. Otherwise, it is an inner particle.

Figure 7 illustrates the complete procedure of implementing the virtual interface method.

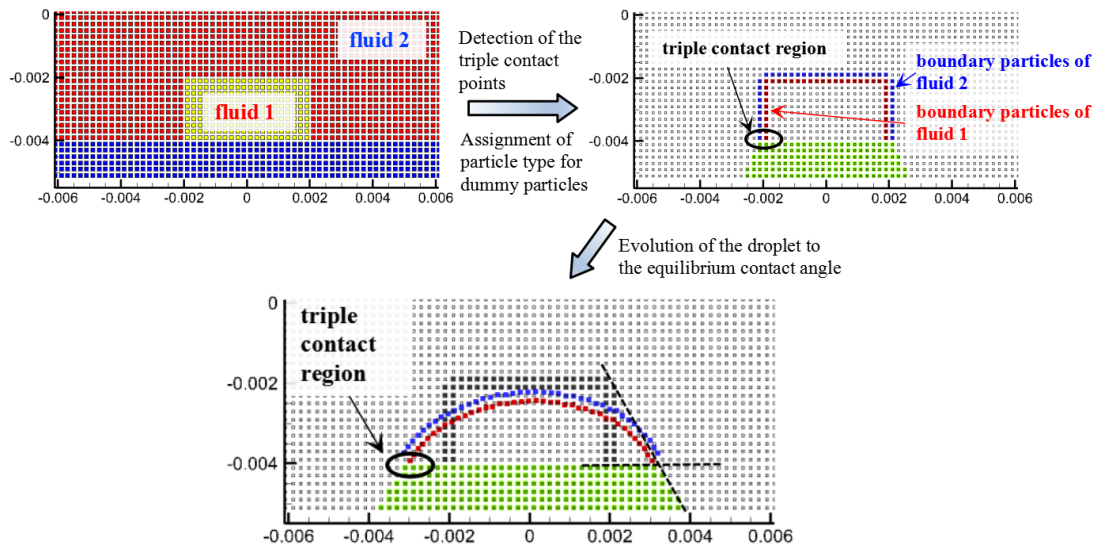


Figure 7 Implementation procedure of the virtual interface method

Figure 8 shows the complete flow chart of the SPH simulation, which is implemented by every time step. .

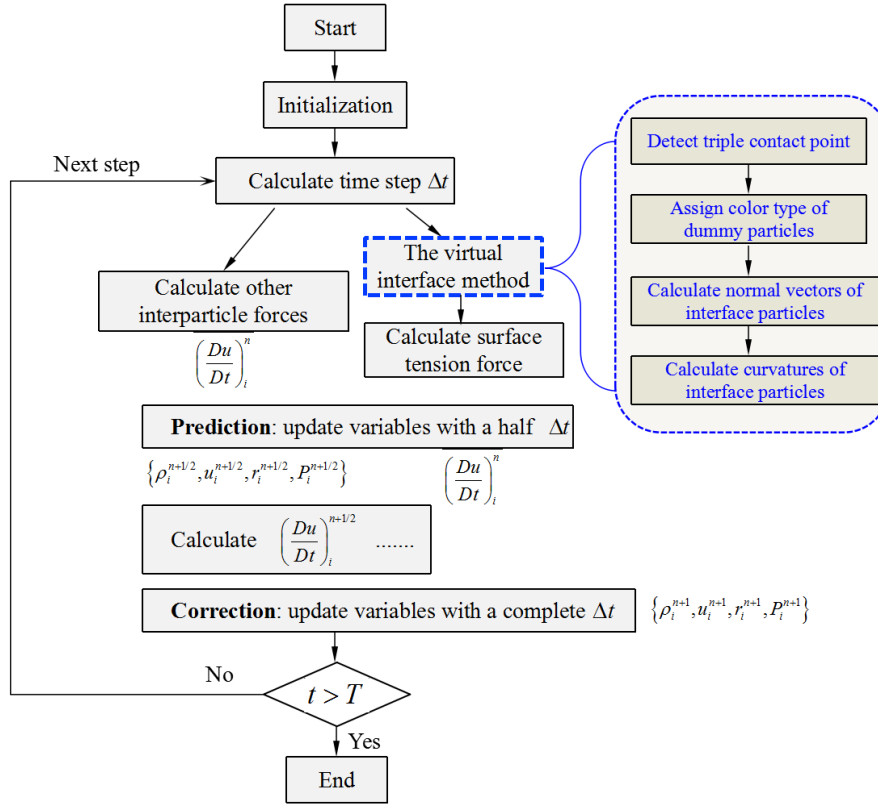


Figure 8 Flow chart of the numerical simulation implemented with the virtual interface method

4. Results and discussion

We consider a droplet deposited on the solid surface and initialized as square shape. Various contact angles can be simulated by changing the input conditions, i.e., the equilibrium contact angles. The simulation domain is a rectangular box of dimensions $L_x \times L_y$ discretized by different resolutions. At the bottom center, a rectangular region of $l_x \times l_y$ is assigned to fluid 1 (liquid), while the surrounding particles are assigned to fluid 2 (gas). The fluid phases include water (liquid) and air (gas). The material properties of liquid and gas are set according to water and air, where the density ratio is 1000.0, the viscosity ratio is 10.0, and the surface tension coefficient is set as 0.072 N/m.

4.1 Evolution of liquid lumps towards the equilibrium contact angle

We first investigate the evolution of the initially square liquid lump. The equilibrium contact angle is set as $\theta_{eq} = 60^\circ$. As shown in Figure 9, the sharp corners become smoothed under the effect of the surface tension. At the same time, the droplet is stretched outwards due to the adjusting force of contact angle. During the evolution process, the position of the triple contact point continually changes, so the color distribution of the dummy particles also varies with time. The droplet experiences a period of oscillation until it evolves to the equilibrium contact angle. From the last picture of Figure 9 one can see that the tangential line of the liquid-gas interface at the triple contact point is visually coincided with the desired contact line, which illustrates that the contact angle method works.

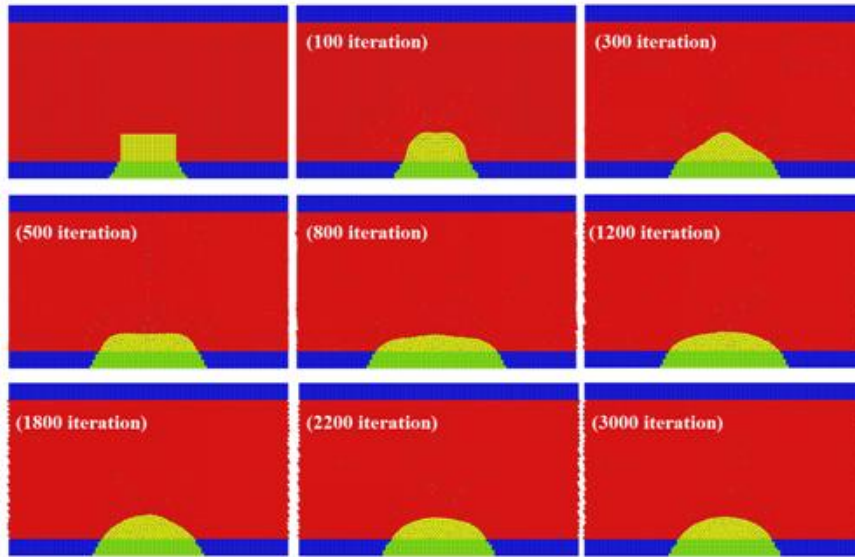
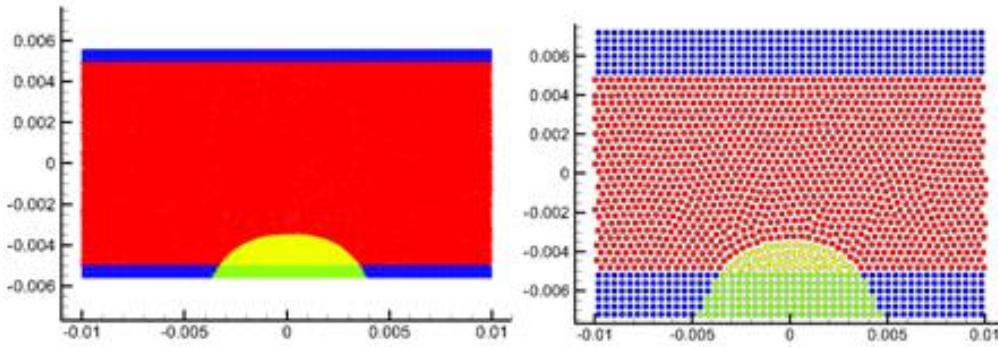


Figure 9 Evolution of a liquid lump to the equilibrium contact angle. (Particle spacing: 100×50 , $\theta_{eq} = 60^\circ$)



(a) Particle spacing: 200×100

(b) Particle spacing: 50×25

Figure 10 Simulation using different particle spacing. ($\theta_{eq} = 60^\circ$)

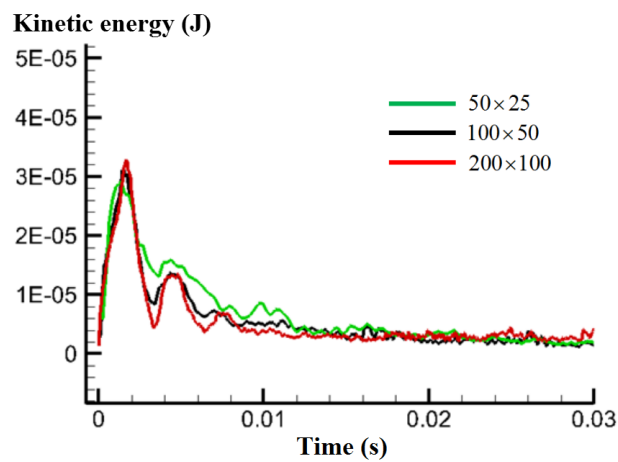


Figure 11 Time history of the kinetic energy of the droplet

Then, we compare the results with different particle spacings, as shown in [Figure 10](#). It illustrates that the final droplet morphology is insignificantly influenced by the particle

spacing. Figure 11 shows the time history of the kinetic energy of the droplet during the simulation. At early stages, the kinetic energy reaches to the peak value because both the surface tension and adjusting force have the largest values. At approximately $t=0.01s$ circular droplet is formed and the particles are nearly at rest, *i.e.* the kinetic energy is very low. For different particle spacings the curve of kinetic energy generally have the same pattern, but the oscillation magnitude increases with the decrease of particle spacing. That is probably because the adjusting force of contact angle is dependent on the particle spacing.

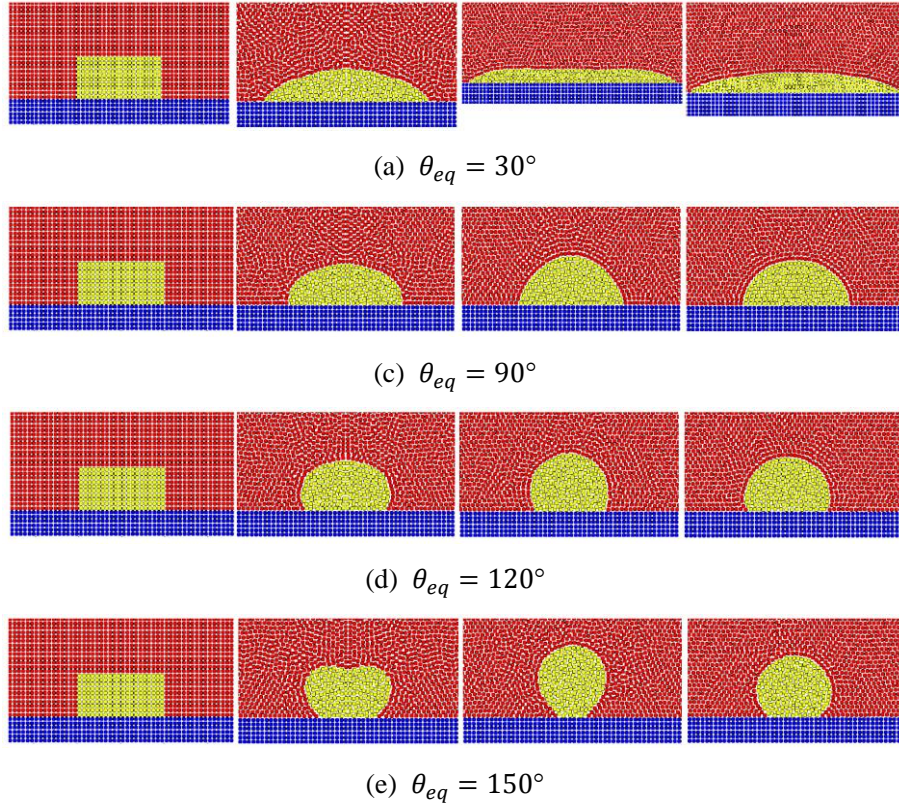


Figure12. Evolution of liquid droplet on a smoothed surface with various contact angles

Then, various contact angles from 30° to 150° are tested. As shown in Figure 12, all presented cases are given the same initial configurations except the input contact angles.

4.2 2D Droplet morphology on the smooth surface

In this section, we first validate the proposed simulation method by considering the morphology of a 2D droplet deposited on the smooth surface.

The analytical solution of 2D droplet morphology had been derived by Liu and Xia^[36] based on the classical Laplace equation across the liquid-gas interface. As shown in Figure 1, the radius of the liquid-solid area is defined as a , the maximum height of the droplet is h_{drop} . The boundary conditions of the semi-droplet are expressed as:

$$y(0) = h_{drop}, y'(0) = h_{drop}, \quad (22)$$

$$y(a) = 0, y'(a) = -\tan \theta_{eq}, \quad (23)$$

The volume of the droplet is given as

$$S = \int_{-a}^a y dx, \quad (24)$$

The analytical solution of the dimensionless morphology for the droplet can be obtained from Eqs. (24) and (25) [36], in which the effects of gravity, surface tension, hydrostatic pressure and transversality condition are considered.

$$\kappa x = 2[E(k_0, \varphi) - E(k_0, \varphi_0)] - [F(k_0, \varphi) - F(k_0, \varphi_0)], \quad (25)$$

$$\kappa y = c_0 \kappa^{-1} - 2k_0 \cos \varphi, \quad (26)$$

where $\kappa^{-1} = \sqrt{\sigma/(\rho g)}$ is the capillary length, x, y are the coordinates of droplet surface, $E(k_0, \varphi)$ and $F(k_0, \varphi)$ are the elliptic integrals of the first and second kinds, c_0 is the curvature at the triple contact point, k_0 is the variable which is determined according to the boundary condition. In the Eqs. (24) and (25), the droplet morphology is expressed as the function of the variable φ , while the variable k_0 can be computed from the boundary condition. Parameters including θ_{eq} , c_0 , and κ^{-1} are taken as input parameters.

In this section, a range of simulations are carried out by changing the input conditions of droplet volume and contact angle θ_{eq} . The volume of the droplet can be expressed as $l_x \times l_y$. When the simulation reaches quasi-static state, *i.e.*, the droplet shape changes slightly with time, the droplet morphology is extracted from the particle distribution. As an example, Figure 13 shows the particle distributions of the fluid system when the droplet is in equilibrium state, and the analytical solution of liquid-gas interface is also plotted in the Figure.

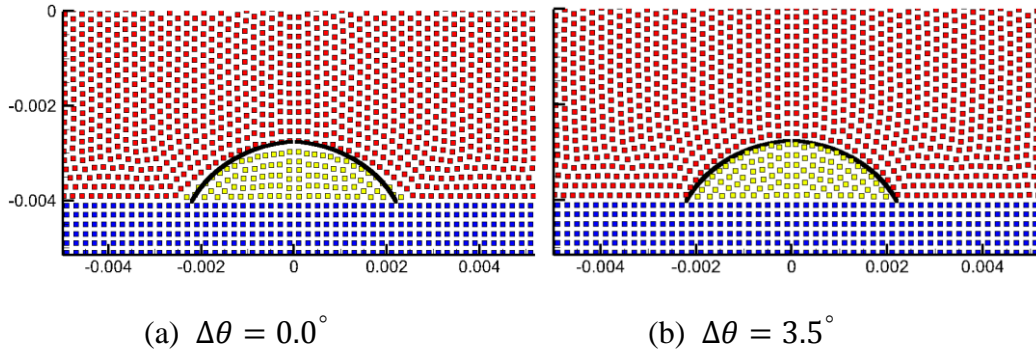


Figure 13 Particle distribution at the equilibrium contact angle. Solid line represents the analytical solution of droplet morphology ($\kappa^{-1} = 0.0027$, $l_x \times l_y = 2.6 \times 1.3$ mm, $\theta_{eq} = 60^\circ$)

If the input contact angle (θ'_{eq}) is set equal to the desired contact angle (θ_{eq}), as shown in Figure 13(a), the simulated contact angle is always smaller than the desired value, so that the predicted droplet morphology is not accurately consistent with the analytical result. It indicates that the adjusting force is inadequate to accurately calibrate the contact line. Therefore, we introduce a correction angle to correct the input value of contact angle as:

$$\theta'_{eq} = \theta_{eq} + \Delta\theta, \quad \Delta\theta > 0^\circ \quad (27)$$

where $\Delta\theta$ is the correction angle. θ'_{eq} is the actual input contact angle substituting θ_{eq} . We investigate several cases for various contact angles from 30deg to 150deg, and find that accurate results of the simulated contact angles can be obtained by setting the $\Delta\theta$ between

3° and 5°.

As shown in Figure 13(b), the predicted result of droplet shape is match every well with the analytical result on the condition that the equilibrium contact angle is accurately implemented. Figure 14 shows the comparison of droplet outlines between analytical results and SPH results. It can be seen from Figure 14 that there are good agreements of droplet outlines between SPH results and analytical solutions.

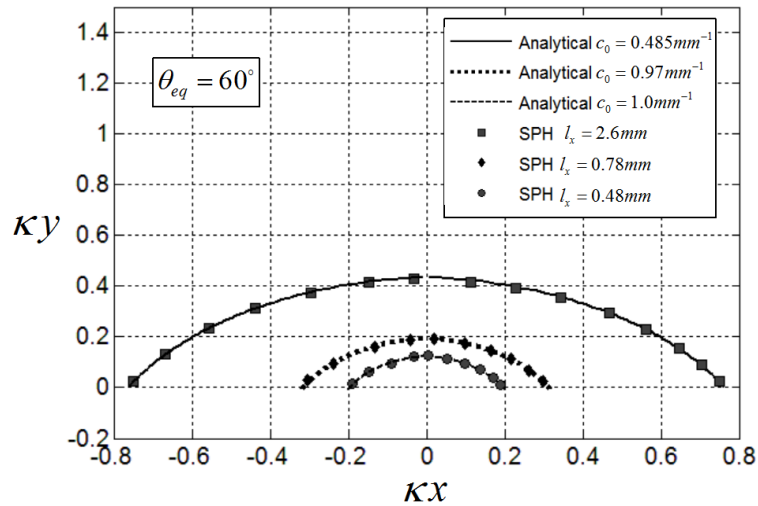


Figure 14 Comparison of droplet morphology between SPH results and analytical results ($\kappa^{-1} = 0.0027$)

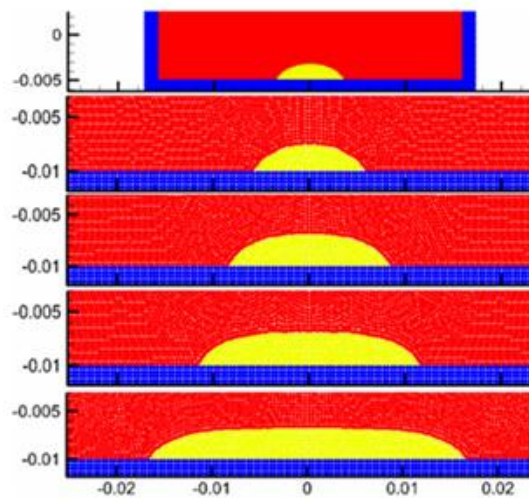


Figure 15 The shape of the droplets changes as the size gets larger ($\theta_{eq} = 60^\circ, \kappa^{-1} = 0.0027m$)

Figure 15 shows the predicted droplet morphologies for various droplet volumes and constant contact angle of 60°. As shown in the Figure, when the volume of the droplet is small, the curvature of the top of the droplet is relatively large, and the radius of curvature is small, so that the droplet shape is close to a sphere. As the volume of the droplet gradually increases, its shape gets far away from the sphere.

4.3 Droplet morphology on a solid surface with sinusoidal microstructures

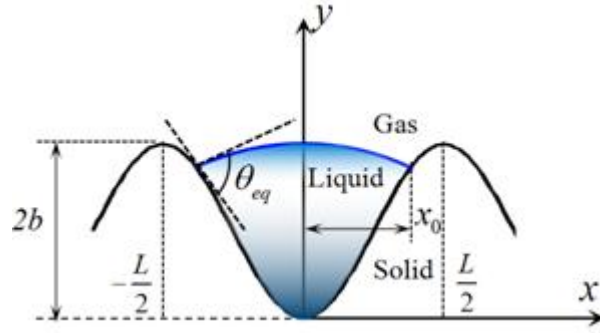


Figure 16 A droplet on a sinusoidal substrate

This section aims to test the applicability of the contact angle method on curved surfaces. As an example, we analyze a single droplet on a sinusoidal surface, as shown in Figure 16. The substrate surface shape is expressed as:

$$y(x) = b[1 - \cos(qx)] \quad (28)$$

where $2b$ is the roughness amplitude, $q = 2\pi/L$ the wave number, and L the wavelength.

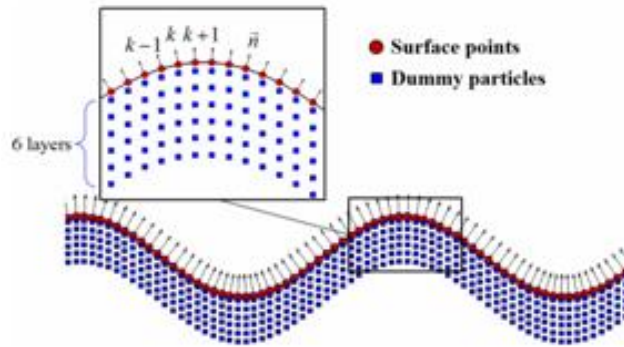


Figure 17 Dummy particles for the rough surface substrate

For the simulation of solid boundary with curved surface substrate, as shown in Figure 17, a set of uniformly distributed surface points are created along the surface first. The surface vectors at an arbitrary point k can be calculated by following equations:

$$\mathbf{n}_k = (n_x, n_y) = \left(-\frac{y_{k+1} - y_{k-1}}{|\mathbf{x}_{k+1} - \mathbf{x}_{k-1}|}, \frac{x_{k+1} - x_{k-1}}{|\mathbf{x}_{k+1} - \mathbf{x}_{k-1}|} \right) \quad (29)$$

$$\boldsymbol{\tau}_k = (\tau_x, \tau_y) = \left(\frac{x_{k+1} - x_{k-1}}{|\mathbf{x}_{k+1} - \mathbf{x}_{k-1}|}, \frac{y_{k+1} - y_{k-1}}{|\mathbf{x}_{k+1} - \mathbf{x}_{k-1}|} \right) \quad (30)$$

where $k, k-1, k+1$ represent surface points of the solid surface adjacent to each other, $\mathbf{n}_k, \boldsymbol{\tau}_k$ are the normal unit vector and tangential unit vector at point k , \mathbf{x}_k is position vector of the point k .

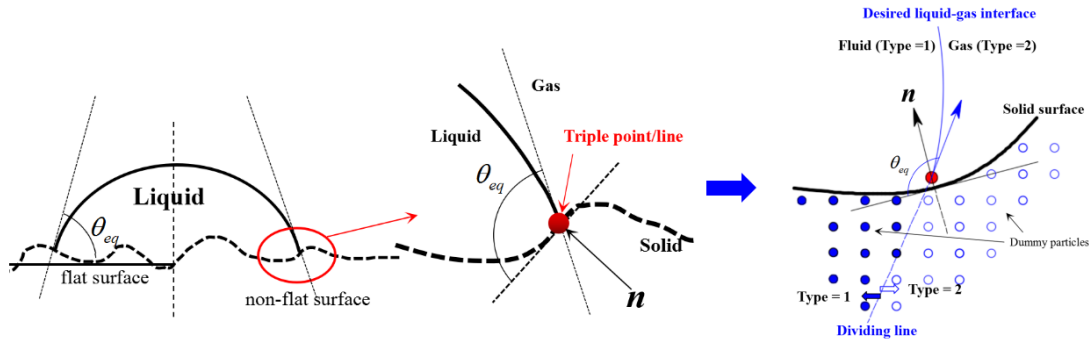


Figure18. The treatment of solid boundary for a curved surface

Let us first consider the case where the droplet is deposited in the single groove. The droplet is still initialized as a square lump, similar to the way we did for smooth surface. The domain is $0.02 \times 0.005\text{m}$ in the rectangular region using a fixed particle initial spacing $d_{ini} = 0.0001$.

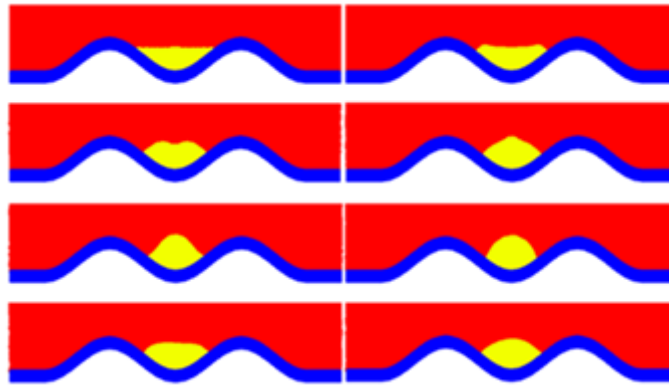


Figure 19 Evolution of liquid droplet in the single groove ($b = 1.0\text{mm}$, $L = 8\text{mm}$, $l_x = 5.2\text{mm}$, $\theta_{eq} = 80^\circ$)

As shown in Figure 18, the droplet is initially in non-equilibrium state. It begins to deform under the action of gravity, surface tension, and contact angle adjusting force. The surface tension causes the sharp corners of the droplet shape to get smoothed. The contact angle adjusting force acts on the fluid near the triple line, causing the droplet to evolve toward the desired contact angle.

As shown in Figure 19, the steady-state morphology of droplets are obtained using different input contact angles in case b, and the color distributions of the dummy particles at steady state are also shown. Consider a droplet located on a rough or curved solid whose characteristic size of surface roughness is of the same order as the droplet size. Then the model can be applied to simulate the droplet morphology. For example, some results of droplet shapes on the sinusoidal surface of case b are plotted in Figure 25. The wavelength L of the roughness is taken as $b = 1\text{mm}$ and the contact angle $\theta_{eq} = 60^\circ$. The color distribution of the dummy particle is also given at each moment, which shows that and the color distribution of dummy particle color changes with the movement of the droplet.

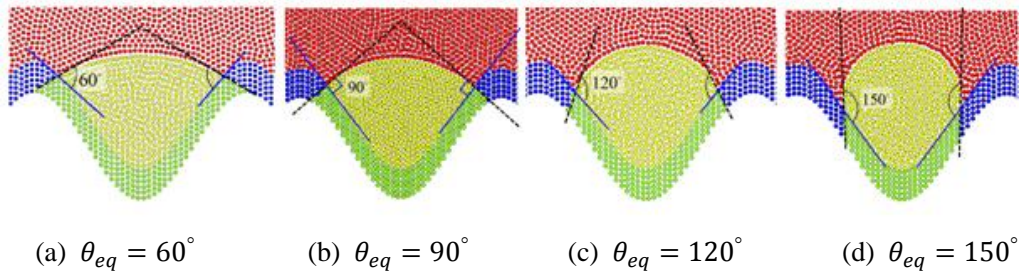


Figure 20 Color distributions of dummy particles for various contact angles ($b = 1\text{mm}$, $L = 3.63\text{mm}$)

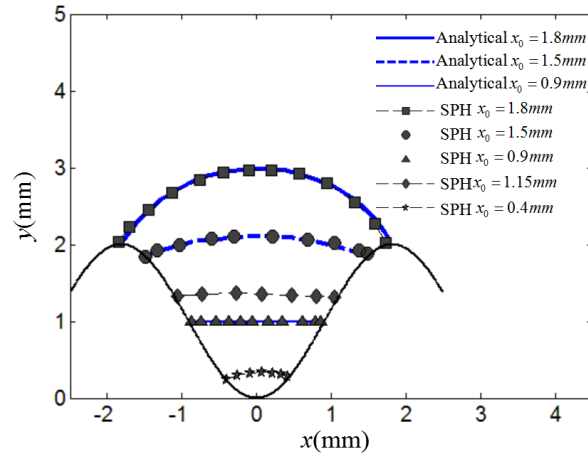


Figure 21 Comparison of droplet morphology between SPH results and analytical results ($\kappa^{-1} = 0.0027$)

For validation, some solutions of droplet shapes on a sinusoidal hydrophilic surface are plotted in Figure 21 for the wavelength $L = 3.63\text{mm}$, the height of the roughness $a = 1\text{mm}$, and the contact angle $\theta_{eq} = 60^\circ$. The analytical solutions from the reference [35] are also plotted in Figure 21. It shows the SPH results are in good agreement with the analytical solutions for three comparative cases of $x_0 = 1.8\text{mm}$, 1.5mm , and 0.9mm . It also can be seen from the Figure that the droplet shape is sensitive to the characteristic size of roughness and the contact angle.

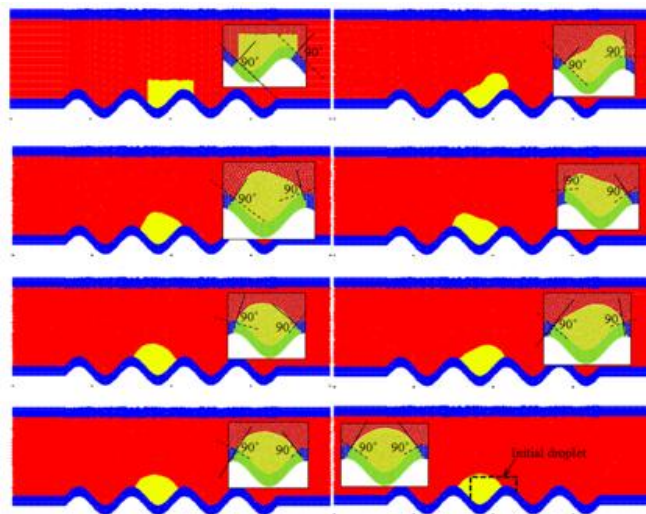


Figure 22 Evolution of liquid droplet on a non-smoothed surface ($b = 0.5\text{mm}$,

$$L = 3.63\text{mm}, \theta_{eq} = 90^\circ)$$

As shown in Figure 22, the liquid lump is initially placed offset from the center of the groove. Under the effects of several forces, the liquid lump move to the left as a whole until it arrives at the center of the groove. During this process, the droplet with smooth surface is gradually formed. The adjusting force calibrates the distribution of fluid near the triple line. Finally, the droplet is settled down in the single groove with the desired contact angle $\theta_{eq} = 90^\circ$.

Above results show that the proposed contact angle method is suitable for the rough surface whose characteristic size is of the same order as the droplet size.

5. Summary

In this paper, based on the SPH multiphase flow algorithm and the CSF surface tension model, a method of implementing contact angle is proposed to simulate the droplet morphology on smooth surface and roughness surface substrates. The results can be summarized as follows:

1. The virtual interface method is proposed to implement contact angle in SPH multiphase simulation. It requires two critical steps: (a) Identifying the triple contact points through searching the boundary particles of each fluid phase; (b) Dividing the dummy particles into two types by the desired contact line. Then, the virtual liquid-gas interface can be created from the triple contact point to the inside of solid wall.

2. The adjusting force is defined as the function of interface curvature and normal unit vector. By means of the virtual liquid-gas interface, the adjusting force which is distributed into the fluid particles near the triple line, always tends to calibrate the dynamic line towards the equilibrium contact angle.

3. The proposed contact angle method is validated for simulations of contact angles on a smooth surface and a roughness surface with sinusoidal microstructures. A initially square liquid lump can evolve towards the equilibrium droplet morphology with the desired contact angle. The predicted droplet shapes are in good agreement with the analytical solutions. In future work, the contact angle scheme for three dimensional model will be considered.

Reference

- 1 de Gans B J, Duineveld P C, Schubert U S. Inkjet printing of polymers: state of the art and future developments[J]. *Advanced materials*, 2004, 16(3): 203-213.
- 2 Goldszal A, Bousquet J. Wet agglomeration of powders: from physics toward process optimization[J]. *Powder Technology*, 2001, 117(3): 221-231.
- 3 Squires T M, Quake S R. Microfluidics: Fluid physics at the nanoliter scale[J]. *Reviews of modern physics*, 2005, 77(3): 977.
- 4 Sun M, Luo C, Xu L, et al. Artificial lotus leaf by nanocasting[J]. *Langmuir*, 2005, 21(19): 8978-8981.
- 5 Pate J S, Atkins C A, White S T, et al. Nitrogen nutrition and xylem transport of nitrogen in ureide-producing grain legumes[J]. *Plant Physiology*, 1980, 65(5): 961-965.
- 6 Gao X, Jiang L. Biophysics: water-repellent legs of water striders[J]. *Nature*, 2004, 432(7013): 36-36.
- 7 Hirt C W, Nichols B D. Volume of fluid (VOF) method for the dynamics of free boundaries[J]. *Journal of computational physics*, 1981, 39(1): 201-225.
- 8 Liu G R, Liu M B. Smoothed particle hydrodynamics: a meshfree particle method[M]. World Scientific, 2003.
- 9 Gingold R A, Monaghan J J. Smoothed particle hydrodynamics: theory and application to non-spherical stars[J]. *Monthly notices of the royal astronomical society*, 1977, 181(3): 375-389.
- 10 Monaghan J J. Simulating free surface flows with SPH[J]. *Journal of computational physics*, 1994, 110(2): 399-406.
- 11 Randles P W, Libersky L D. Smoothed particle hydrodynamics: some recent improvements and

- applications[J]. *Computer methods in applied mechanics and engineering*, 1996, 139(1-4): 375-408.
- 12 Hu X Y, Adams N A. A multi-phase SPH method for macroscopic and mesoscopic flows[J]. *Journal of Computational Physics*, 2006, 213(2): 844-861.
- 13 Ming F R, Sun P N, Zhang A M. Numerical investigation of rising bubbles bursting at a free surface through a multiphase SPH model[J]. *Meccanica*, 2017: 1-20.
- 14 Zhang A, Sun P, Ming F. An SPH modeling of bubble rising and coalescing in three dimensions[J]. *Computer Methods in Applied Mechanics and Engineering*, 2015, 294: 189-209.
- 15 Grenier N, Antuono M, Colagrossi A, et al. An Hamiltonian interface SPH formulation for multi-fluid and free surface flows[J]. *Journal of Computational Physics*, 2009, 228(22): 8380-8393.
- 16 Colagrossi A, Landrini M. Numerical simulation of interfacial flows by smoothed particle hydrodynamics[J]. *Journal of computational physics*, 2003, 191(2): 448-475.
- 17 Adami S, Hu X Y, Adams N A. A new surface-tension formulation for multi-phase SPH using a reproducing divergence approximation[J]. *Journal of Computational Physics*, 2010, 229(13): 5011-5021.
- 18 Szewc K, Pozorski J, Minier J P. Simulations of single bubbles rising through viscous liquids using smoothed particle hydrodynamics[J]. *International Journal of Multiphase Flow*, 2013, 50: 98-105.
- 19 Yeganehdoust F, Yaghoubi M, Emdad H, et al. Numerical study of multiphase droplet dynamics and contact angles by smoothed particle hydrodynamics[J]. *Applied Mathematical Modelling*, 2016, 40(19): 8493-8512.
- 20 Nugent S, Posch H A. Liquid drops and surface tension with smoothed particle applied mechanics[J]. *Physical Review E*, 2000, 62(4): 4968.
- 21 Tartakovsky A, Meakin P. Modeling of surface tension and contact angles with smoothed particle hydrodynamics[J]. *Physical Review E*, 2005, 72(2): 026301.
- 22 Brackbill J U, Kothe D B, Zemach C. A continuum method for modeling surface tension[J]. *Journal of computational physics*, 1992, 100(2): 335-354.
- 23 Morris J P. Simulating surface tension with smoothed particle hydrodynamics[J]. *International journal for numerical methods in fluids*, 2000, 33(3): 333-353.
- 24 Liu M B, Liu G R. Meshfree particle simulation of micro channel flows with surface tension[J]. *Computational Mechanics*, 2005, 35(5): 332-341.
- 25 Hu X Y, Adams N A. A multi-phase SPH method for macroscopic and mesoscopic flows[J]. *Journal of Computational Physics*, 2006, 213(2): 844-861.
- 26 Das A K, Das P K. Equilibrium shape and contact angle of sessile drops of different volumes—Computation by SPH and its further improvement by DI[J]. *Chemical Engineering Science*, 2010, 65(13): 4027-4037.
- 27 Wang Z B, Chen R, Wang H, et al. An overview of smoothed particle hydrodynamics for simulating multiphase flow[J]. *Applied Mathematical Modelling*, 2016, 40(23): 9625-9655.
- 28 Breinlinger T, Polfer P, Hashibon A, et al. Surface tension and wetting effects with smoothed particle hydrodynamics[J]. *Journal of Computational Physics*, 2013, 243: 14-27.
- 29 De Gennes P G, Brochard-Wyart F, Quéré D. *Capillarity and wetting phenomena: drops, bubbles, pearls, waves*[M]. Springer Science & Business Media, 2013.
- 30 Morris J P, Fox P J, Zhu Y. Modeling low Reynolds number incompressible flows using SPH[J]. *Journal of computational physics*, 1997, 136(1): 214-226.
- 31 Crespo A J C, Gómez-Gesteira M, Dalrymple R A. Boundary conditions generated by dynamic particles in SPH methods[J]. *CMC-TECH SCIENCE PRESS*, 2007, 5(3): 173.
- 32 Dilts G A. Moving least-squares particle hydrodynamics II: conservation and boundaries[J]. *International Journal for Numerical Methods in Engineering*, 2000, 48(10): 1503-1524.
- 33 Marrone S, Colagrossi A, Antuono M, et al. An accurate SPH modeling of viscous flows around bodies at low and moderate Reynolds numbers[J]. *Journal of Computational Physics*, 2013, 245: 456-475.
- 34 Monaghan J J, Rafiee A. A simple SPH algorithm for multi-fluid flow with high density ratios[J]. *International Journal for Numerical Methods in Fluids*, 2013, 71(5): 537-561.
- 35 Liu J L, Feng X Q, Yu S W. Morphology of liquid drops and thin films on a solid surface with sinusoidal microstructures[J]. *ActaMechanicaSinica*, 2006, 22(4): 315-322.
- 36 Jian-Lin, Liu. A unified analysis of a micro-beam, droplet and CNT ring adhered on a substrate: Calculation of variation with movable boundaries[J]. *Acta Mechanica Sinica*, 2013, 29(1):62-72.

Acknowledgements

This project was supported by China Postdoctoral Science Foundation (Grant NO. 2017M622307). This project was also partially supported by Shandong natural science foundation (Grant NO. ZR201709210320) and Fundamental Research Funds for the Central

Universities (Grant No. 18CX02153A). I also want to give my thanks to Dr. Li-Chenxue, who inspires me to grow up, mentally and intellectually.